Ferroelectricity in strained $Ca_{0.5}Sr_{0.5}TiO_3$ from first principles

Christopher R. Ashman
1602 W. 42nd Street, Richmond, Virginia 23225, USA

C. Stephen Hellberg
Center for Computational Materials Science Code 6393, Naval Research Laboratory, Washington, DC 20375, USA

Samed Halilov
Department of Materials Science and Engineering, MIT, 77 Massachusetts Avenue, Cambridge, Massachusetts 02139, USA

(Received 1 April 2010; revised manuscript received 6 July 2010; published 28 July 2010)

We present a density-functional theory investigation of strained $Ca_{0.5}Sr_{0.5}TiO_3$ (CSTO). We have determined the structure and polarization for a number of arrangements of Ca and Sr in a $2\times2\times2$ supercell. The *a* and *b* lattice vectors are strained to match the lattice constants of the rotated Si(001) face. To set the context for the CSTO study, we also include simulations of the Si(001) constrained structures for $CaTiO_3$ and $SrTiO_3$. Our primary findings are that all $Ca_{0.5}Sr_{0.5}TiO_3$ structures examined except one are ferroelectric, exhibiting polarizations ranging from 0.08 C/m^2 for the lowest energy configuration to about 0.26 C/m^2 for the higher energy configurations. We find that the configurations with larger polarizations have lower c/a ratios. The net polarization of the cell is the result of Ti-O ferroelectric displacements regulated by *A*-site cations.

DOI: 10.1103/PhysRevB.82.024112 PACS number(s): 77.80.bg, 61.50.Ah, 77.80.bn, 81.05.Zx

There is great interest in combining ferroelectrics (FEs) with semiconductors. Potential devices include nonvolatile memory, reprogrammable logic, and even quantum computation.[1] Ideally, ferroelectrics would be grown on the technologically dominant Si(001) surface, and there has been great effort at growing $SrTiO_3$ (STO) on Si(001).[2–7] The in-plane lattice parameters of $SrTiO_3$ are 1.7% larger than those of the (110) and (110) directions of the Si(001) surface, and thin films of compressively strained STO have been shown to exhibit the desired ferroelectric behavior.[5,7] However, as the thickness of the film increases, the STO relaxes to the unstrained state and the ferroelectric behavior is no longer observed.[4,7] One possibility to induce ferroelectricity into $SrTiO_3$ films is to introduce dopants such as either Ba or Ca.[8–10] For example, $Ca_{(1-x)}Sr_xTiO_3$ offers the possibility of invoking ferroelectricity in $SrTiO_3$ while at the same time maintaining a closer lattice match to the Si(001) surface. Although there have been a number of experimental studies aimed at identifying the crystal structure and lattice properties of unstrained $Ca_{(1-x)}Sr_xTiO_3$,[11–13] to date the authors are not aware of any theoretical studies of the strained case.

In this work we present a theoretical study of ferroelectrically induced polarization in bulk, strained $Ca_{0.5}Sr_{0.5}TiO_3$. Structural optimizations were done using the VASP code[14,15] with the projector augmented wave method to treat the electronic structure problem.[16] The gradient corrected exchange-correlation (XC) functionals were treated within the Perdew, Becke, and Ernzerhof scheme.[17] In all cases we used a supercell consisting of $2\times2\times2$ primitive cells or two layers of four primitive cells each. This requires eight alkaline-earth atoms in the unit cell while allowing for the inclusion of rotation and tilting effects in the oxygen octahedra. Periodic boundary conditions were employed to simulate a spatially extended material. We used a $4\times4\times4$ *k*-point mesh and a plane-wave cutoff energy of 350 eV. The unit cell was strained to match the lattice constants of the 45° rotated Si(001) face. For our unit cell the **a** and **b** lattice vectors are 7.728 Å. The **c** lattice vector is obtained by calculating the total energy for a range of values separated by 0.01 Å approximately centered on the cubic value until a minimum-energy configuration was bracketed. For the total-energy calculations the lattice parameters were frozen but the atomic positions were free to relax until the forces were smaller than 0.005 eV/Å along any Cartesian direction for any atom.

For the calculation of polarization we used the ABINIT code[18] and FHI98 pseudopotentials of the Trouiller-Martins type.[19] The structure was imported directly from the VASP code structural optimization step and no relaxation was performed for the lattice or ions.

In the chosen unit cell there are eight *A* sites (alkaline earth) of which four are occupied by Ca and four by Sr. Most of the 70 possible arrangements of the cations are related by rotational and mirror symmetries. We examined the nine configurations shown in Fig. 1.

Our primary result is that all the configurations we considered except one exhibit a net ferroelectric dipole moment. The lowest energy configuration consists of alternating stripes of Ca and Sr running diagonally across the strained face of the perovskite. This configuration possesses a net polarization of 0.077 C/m^2. We find that there is a trend for the lowest energy configurations to have the smallest polarizations and the largest c/a ratios. We summarize this information in Table I.

Several studies on $SrTiO_3$ have shown that quantum fluctuations may compete with ferroelectric distortions, leaving the perovskite in an unpolarized state referred to as an incipient ferroelectric.[20,21] To address this possibility in the doped perovskite, we have calculated the energy difference between the polarized and unpolarized cells for the two cases corresponding to the lowest energy configuration (l1ol1xyl2ol2xy) and the alternating stacked sequence of Ca and Sr (l1ol1xl1yl1xy). We find the energy differences to be 0.07 eV/f.u. and 0.03 eV/f.u. (five-atom cell) for the lowest energy configuration and the stacked configuration, respec-

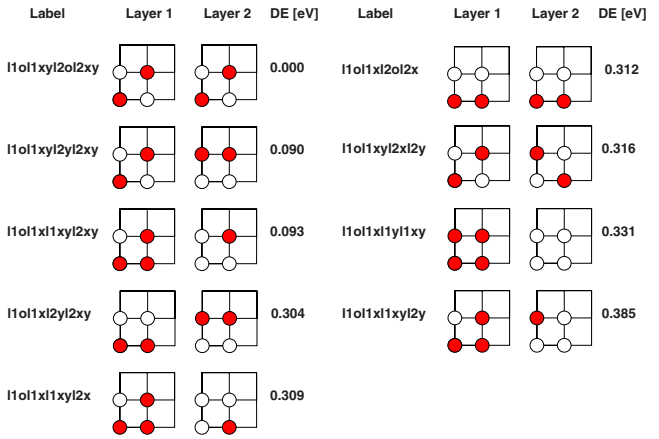

FIG. 1. (Color online) Top view schematic of the configurations considered in this work. The left column is an identification for each configuration, the second column is a schematic of the first layer, the third column is a schematic of the second layer. The final column gives the relative energies. The hollow/filled (white/red) circles represent the positions of the Ca/Sr atoms on the *xy*-plane lattice face.

tively. If we use formula (1) from Ref. 21 to estimate the contribution of quantum fluctuations we come up with about 0.003 eV/oxygen or about 0.01 eV/f.u. Thus it is likely that the polarization in these cells persists.

We find that polarization tends to increase with decreasing c/a ratio. There is an exception to this trend for the configuration labeled l1ol1xl2yl2xy which has no net polarization but has the smallest c/a ratio of those considered. We have plotted the relative energies of the configurations as a function of c/a ratio in Fig. 2. In this figure we label four families of curves which are differentiated based on the antiferrodistortive (AFD) rotations and/or tiltings. The four distinct combinations of rotation and tilting are presented in Fig. 3 which consist of projections down the (100), (010), and (001) faces of the l1ol1xyl2ol2xy, l1ol1xyl2yl2xy, l1ol1xl1xyl2x, and l1ol1xl2yl2xy configurations, respectively. For simplicity of expressing the rotations and tilting of the oxygen octahedra we employ the Glazer notation.[22] This notation was developed for ABX_3 perovskites and assumes rigid rotations of the oxygen octahedral cages whereas we are considering the case of $AA'TiO_3$ and allow distortions of the oxygen cages.

TABLE I. Tabulated data for the configurations at 50% Ca and 50% Sr pictured in Fig. 1. Included are the configuration identification, the total energy, relative energy, and polarization for the lowest energy of each configuration.

$Ca_{1/2}Sr_{1/2}TiO_3$			
Configuration	ΔE (eV)	$\frac{c}{a}$ ratio	Polarization (C/m^2)
l1ol1xyl2ol2xy	0.000	1.043	0.077
l1ol1xyl2yl2xy	0.090	1.048	0.035
l1ol1xl1xyl2xy	0.094	1.048	0.037
l1ol1xl2yl2xy	0.304	1.020	0.000
l1ol1xl1xyl2x	0.309	1.030	0.250
L1ol1xl2ol2x	0.312	1.030	0.245
l1ol1xyl2xl2y	0.316	1.033	0.253
l1ol1xl1yl1xy	0.331	1.030	0.268
l1ol1xl1xyl2y	0.385	1.027	0.031

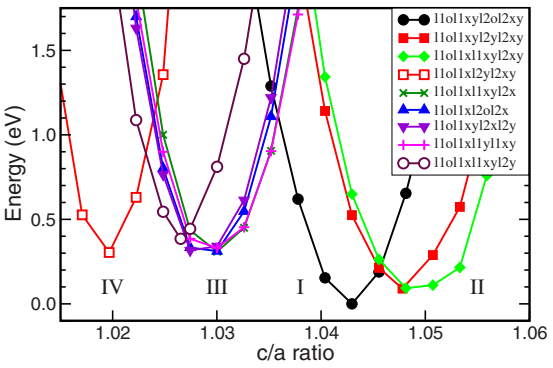

FIG. 2. (Color online) Plot of the relative energy as a function of c/a ratio for the configurations considered in this work. The curves were shifted so that the globally lowest energy configuration aligned with 0.00 eV. The labels I, II, III, and IV correspond to arrangements of $a^+a^+c^-$, $a^+a^+c^0$, $a^-b^+c^-$, and $a^-b^+c^+$ tilting and rotation of the oxygen octahedra.

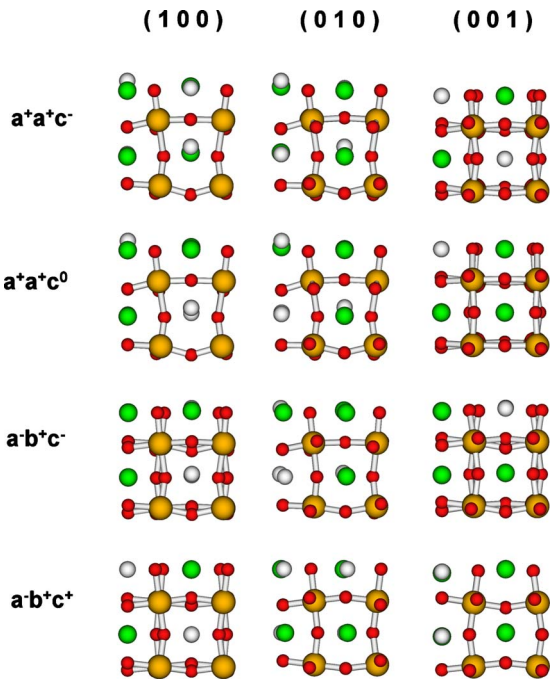

FIG. 3. (Color online) Ball and stick models of the lowest energy configuration corresponding to each combination of AFD rotations and tilting of the oxygen octahedra exhibited by configurations investigated in this work. We present views down the (100), (010), and (001) planes, respectively. The models correspond to the configurations lying at the bottoms of the curves labeled in Fig. 1. In order from smallest to largest balls, the O are red, Ca white Sr green, and Ti yellow.

TABLE II. Tabulated data for the A=l1ol1xyl2ol2xy, B=l1ol1xyl2xl2y, and C=l1ol1xl1yl1xy configurations at 50% Ca and 50% Sr pictured in Fig. 1. The first two columns are the difference in energy between the given configuration and the ground state (relative energy) and the c/a ratio for the configurations with no rotations or tilting and no FE displacements of the atoms in the unit cell. Each of the subsequent sets of three columns give the relative energy, c/a ratio, and cell polarization with only FE displacements, AFD rotations, and tilting about the a axis of the cell.

	Tetragonal unpoled		Tetragonal poled			AFD only			Tilting only		
Configuration	δE (eV)	$\frac{c}{a}$	δE (eV)	$\frac{c}{a}$	μ (C/m^2)	δE (eV)	$\frac{c}{a}$	μ (C/m^2)	δE (eV)	$\frac{c}{a}$	μ (C/m^2)
A	1.438	1.025	0.968	1.067	0.090	0.639	1.042	0.250	0.756	1.053	0.020
B	1.442	1.025	1.034	1.067	0.087	0.646	1.030	0.164	0.749	1.056	0.030
C	1.352	1.025	1.058	1.061	0.035	0.647	1.030	0.162	0.633	1.052	0.070

Analysis of the displacement patterns shows that the tetragonal strain is driven by the AFD octahedral rotations hybridized with the FE displacements rather than by the latter alone. Earlier theoretical work has shown that the introduction of dopants with smaller atomic radii into the A sites is able to drive the tetragonal strain.[23] Thus the distribution of Ca cations determines the rotation of the oxygen cages versus the distortion along the tetragonal (c) axis. On the other hand, the polarization is clearly associated with the FE displacements. We find that FE displacements of the Ti atoms relative to the oxygen cages do not vary widely despite the range of polarizations for the different configurations. For example, the Ti atoms undergo an average FE displacement from their centrosymmetric positions in the oxygen octahedra of 0.213 Å for the l1ol1xyl2ol2xy configuration. This configuration has a polarization of 0.077 C/m^2, whereas the l1ol1xl1yl1xy configuration Ti atoms have an average FE displacement of 0.134 Å while exhibiting the one of the largest net polarizations of 0.268 C/m^2. Instead, we find that displacements of the A-site cations play a significant role in determining the overall polarization of the cell. In the l1ol1xyl2ol2xy configuration, the A-site Ca cations have very large displacements along the c axis. The displacement of these cations is such that the Ca-O dipoles are antialigned with the Ti-associated polarization of the cell. If the Ca ions are shifted to be coplanar with the oxygen atoms in the same atomic layer thus removing their contribution to the polarization in the cell, the polarization increases from 0.077 to 0.186 C/m^2. If all A-site cations are shifted to their nonpolar locations, the polarization increases further to 0.222 C/m^2. In their optimal locations, the Ca ions have large displacements of up to 0.589–0.650 Å in the three lowest energy configurations. Other configurations have Ca-ion displacements of 0.000–0.243 Å. The resulting picture is such that the configurations with the lowest energy, groups I and II in Fig. 3, have the highest tetragonal strain and lowest polarization as featured by the relatively strong a^+a^+-type octahedral rotations. These rotations will be referred to as tiltings hereafter in the text.

We consider the effect of the position within the cell of the atomic arrangements on the stability and polarization by examining the three cases of the lowest energy l1ol1xyl2ol2xy configuration, the l1ol1xyl2xl2y configuration which may be thought of as a rocksalt type structure, and finally the l1ol1xl1yl1xy configuration which is constructed of alternating planes of Ca and Sr ions in the (001) plane. Note that for the l1ol1xyl2ol2xy and l1ol1xyl2xl2y configurations, the sequence of the A and A' cations (A=Ca,A'=Sr) along the (**a**,**b**) lattice directions is A-A'- and so on while that of the l1ol1xl1yl1xy is either A-A- or A'-A'-. Along the **c** lattice direction, the l1ol1xyl2ol2xy give either a stacking of A-A- or A'-A'- whereas the other two give A-A'- and so on. Considering these cations as hard spheres, the packing of A-A'- is more compact than that of A'-A'- in the ideal tetragonal structure since the Ca ion is smaller than the Sr ion. We have confirmed that the l1ol1xyl2ol2xy and l1ol1xyl2xl2y undergo smaller compressive strains of (0.5%, 0.5%), and (0.9%, 0.7%) compared to (1.2%, 0.7%) for the l1ol1xl1yl1xy configuration along the **a** and **b** lattice directions. This results in reduced polar AFD rotations. For the l1ol1xyl2ol2xy configuration, the average octahedral rotation about the tetragonal axis is 5.7° while the l1ol1xl1yl1xy configuration has an average octahedral rotation of about 7.7°. In the **c** direction, both the l1ol1xyl2xl2y and l1ol1xl1yl1xy are more compact than the l1ol1xyl2ol2xy which restricts the range of displacements that the Ca ions are permitted. This in turn reduces their ability to respond to the internal electric field established by FE distortions.

To assist in understanding how doping affects the stability and polarization of the perovskite we have performed a series of calculations in which we include only the effects of FE displacements, FE displacements coupled with AFD rotations, and FE displacements coupled with octahedral tilting about one axis. The results are presented in Table II. We find that freezing out the tilting and allowing only AFD rotations of the octahedra coincides with an increase in the cell polarization relative to the case where only FE displacements are allowed, contrary to what is found for STO.[24] This behavior is the result of large ~0.5 Å displacements of the Ca atoms out of the (001) plane of the oxygen atoms in the case where the AFD distortions are suppressed. The Ca atoms are displaced such that the Ca associated electric dipole opposes the contribution from the Ti associated polarization. This is facilitated by a large c/a ratio for the structure. When AFD rotations are included the strain on the octahedral cages is reduced and the tetragonal distortion is smaller. In this case the Ca atom displacements are reduced to about 0.1 Å due to the steric hindrance of the oxygen atoms. Thus their asso-

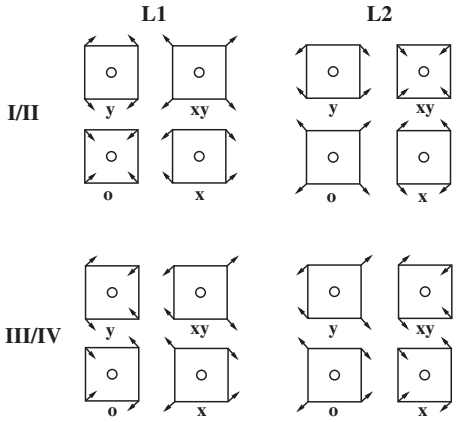

FIG. 4. Schematic diagrams of the (001)-plane projected tilting of the oxygen atoms surrounding the *A*-site cations. The top set of eight panels show the direction of oxygen displacements corresponding to curves I and II of Fig. 2. The bottom set corresponds to those of curves III and IV. In each case, the left four panels are for layer 1 (L1) and the right set are for layer 2 (L2). Each schematic is labeled with an o, x, y, or xy to indicate its proximate placement in the unit cell. Cells adjacent to each other share oxygen atoms and direction vectors indicate that.

ciated electric dipole is of a smaller magnitude.

The inclusion of tilting without AFD rotations also acts to reduce the cell polarization. Due to the compressive strain imposed in the plane, the oxygen octahedra are compressed and there is a large tetragonal distortion out of plane which allows for displacement of the Ca atoms. The distance between the Ca atoms and the nearest oxygen atoms in the Ti-O plane above them (relative to oxygen octahedra that are displaced downward due to polarization effects) is about 2.43 Å as compared to the sum of the ionic radii of Ca and O which is about 2.38–2.42 Å assuming Shannon ionic radii.[25] Thus they are bounded in their displacement primarily by the size of the O and Ca ionic shells. For comparison, the sum of the ionic radii of Sr and O is 2.56–2.60 Å. Generally speaking, the *A*-site cations exhibit distances to nearest-neighbor oxygen atoms from adjacent Ti-O planes that correspond to within 0.05 Å of the sum of their ionic radii.

Based on these observations, the placement of the Ca and Sr atoms in the lattice can be explained. Figure 4 consists of two sets of schematics indicating only the directions of the displacements of the *A*-site planar oxygen atoms relative to the *A*-site cations due to tilting of the octahedral cages. Note that the four sets of curves in Fig. 2 reduce to the two sets of oxygen displacement schematics (including rotation about the *c* axis gives the complete four sets of curves). A study of the figure indicates that once the displacement of the oxygen atoms about one cation have been established, the displacements of all oxygen atoms in the unit cell is specified, assuming rigid oxygen octahedra.

In layer 1 (L1) of Fig. 4 top set of schematics, the schematic labeled "o" indicates that all of the nearest-neighbor oxygen atoms that are coplanar with the *A*-site cation are tilted toward the cation. This set of tiltings corresponds to the large out-of-plane displacements that have been observed for the Ca atoms in the simulations. The lowest energy configurations contain this tilting arrangement. This set of tiltings, coupled with the large *A*-site cation out-of-plane displacements, is associated with the lowest energy configurations. In all nine configurations studied here, no such set of tiltings is associated with the Sr atoms due to their large ionic radii. The tilting drives the *A*-site cations out of the plane. In order for the Sr atoms to displace, the tetragonal distortion must increase with a corresponding increase in strain energy. On the other hand the Ca atoms are able to displace with no additional contribution to the tetragonal strain energy due to their smaller atomic radii. To quantify this, note that, in the l1ol1xyl2ol2xy configuration, the O-O nearest-neighbor separation in *A*-site plane is 3.29 Å. The in-plane distance from one of the oxygen atoms to the center of the square face where a nondisplaced *A*-site cation would reside is 2.33 Å. In order to accommodate a Ca ion, given the ionic radii of the Ca and O, the Ca ion would need to be displaced by about 0.59 Å which is the same as the observed Ca displacement. In order to accommodate an Sr cation, the tetragonal distortion would need to be increased by 0.53 Å per layer.

Given the importance of this octahedral tilting arrangement we are able to explain why the Ca atoms align along (110) planes as opposed to a rocksalt type configuration. Observation of the schematics I/II in Fig. 4 indicates that there can be only one such tilting configuration per layer. These configurations must be staggered diagonally in order not to impose large distortions on the oxygen octahedra. Such an arrangement excludes the rocksalt configuration. It also excludes alternating planes composed of Ca and Sr cations.

TABLE III. Lattice vectors and polarization for Si lattice matched $Ca_{0.5}Sr_{0.5}TiO_3$ (lowest energy configuration), $CaTiO_3$, and $SrTiO_3$ as determined in this work.

Configuration	**a** (Å)	**b** (Å)	**c** (Å)	Polarization (C/m^2)
$Ca_{0.5}Sr_{0.5}TiO_3$	7.728	7.728	8.06	0.077
$CaTiO_3$	7.728	7.728	7.740	0.146
$SrTiO_3$	7.728	7.728	8.136	0.304

In Table III we compare the lattice parameters and polarizations for the Si(001) lattice matched $CaTiO_3$ and $SrTiO_3$ with the lowest energy configuration of $Ca_{0.5}Sr_{0.5}TiO_3$. The c/a ratios sandwich the $Ca_{0.5}Sr_{0.5}TiO_3$ value of 1.043 with 1.002 and 1.053, respectively, and with respect to the 40-atom cell. We find that the mixed configuration has the lowest net polarization. Both $CaTiO_3$ and $SrTiO_3$ are considered incipient ferroelectrics in their unstrained states but have been found to be polar in their strained configurations.[26,27] The oxygen cage rotations may be classified as $a^+b^-c^-$ and $a^0a^0c^-$ for the $CaTiO_3$ and $SrTiO_3$, respectively. In these pure ABO_3 perovskites the *A*-site cations have smaller FE displacements than in the mixed case.

In summary we have identified a ground-state configuration for the Si(001) lattice matched $Ca_{0.5}Sr_{0.5}TiO_3$. This consists of alternating planes of Ca and Sr running along the (110) direction relative to the cubic ABO_3 perovskite phase. We find this structure to be ferroelectric with a net polariza-

tion of 0.077 C/m^2 and a reduced surface strain compared to STO. We have identified eight higher energy configurations which, with one exception, exhibit net ferroelectric polarizations. The *A*-site cations counter the dominant ferroelectric contributions of the Ti atoms. This work shows that the small ionic radius of the Ca ions combined with octahedral rotations allows them to displace in such a way as to minimize the net cell polarization. The placement of the *A*-site cations determines whether AFD rotations or tilting effects are dominant. The former suppresses octahedral distortions and subsequent displacement of the *A*-site cations. When tilting is dominant, the tetragonal distortion is enhanced and the cell polarization decreases.

The present study does not include surface and interface effects which very likely play an important role in both the overall structure and polarization of thin-film structures. However, it identifies the key interactions which govern the stability and polarization of $AA'TiO_3$ perovskites which should prove valuable in designing such materials.

Computations were performed at the AFRL DoD Major Shared Resource Center.

[1] J. Levy, Phys. Status Solidi B **233**, 467 (2002).
[2] C. J. Först, C. R. Ashman, K. Schwarz, and P. E. Blöchl, Nature (London) **427**, 53 (2004).
[3] R. A. McKee, F. J. Walker, and M. F. Chisholm, Phys. Rev. Lett. **81**, 3014 (1998).
[4] J. C. Woicik, H. Li, P. Zschack, E. Karapetrova, P. Ryan, C. R. Ashman, and C. S. Hellberg, Phys. Rev. B **73**, 024112 (2006).
[5] J. C. Woicik, E. L. Shirley, C. S. Hellberg, K. E. Anderson, S. Sambasivan, D. A. Fischer, B. D. Chapman, E. A. Stern, P. Ryan, D. L. Ederer, and H. Li, Phys. Rev. B **75**, 140103 (2007).
[6] L. F. Kourkoutis, C. S. Hellberg, V. Vaithyanathan, H. Li, M. K. Parker, K. E. Andersen, D. G. Schlom, and D. A. Muller, Phys. Rev. Lett. **100**, 036101 (2008).
[7] M. P. Warusawithana, C. Cen, C. R. Sleasman, J. C. Woicik, Y. Li, L. F. Kourkoutis, J. A. Klug, H. Li, P. Ryan, L.-P. Wang, M. Bedzyk, D. A. Muller, L.-Q. Chen, J. Levy, and D. Schlom, Science **324**, 367 (2009).
[8] W. Kleemann, J. Dec, Y. G. Wang, P. Lehnen, and S. A. Prosandeev, J. Phys. Chem. Solids **61**, 167 (2000).
[9] J. G. Bednorz and K. A. Müller, Phys. Rev. Lett. **52**, 2289 (1984).
[10] G. Geneste and J.-M. Kiat, Phys. Rev. B **77**, 174101 (2008).
[11] M. A. Carpenter, C. J. Howard, K. S. Knight, and Z. Zhang, J. Phys. Condens. Matter **18**, 10725 (2006).
[12] D. I. Woodward, P. L. Wise, W. E. Lee, and I. M. Reaney, J. Phys. Condens. Matter **18**, 2401 (2006).
[13] Q. Hui, M. T. Dove, M. G. Tucker, S. A. T. Redfern, and D. A. Keen, J. Phys. Condens. Matter **19**, 335214 (2007).
[14] G. Kresse and J. Hafner, Phys. Rev. B **47**, 558 (1993).
[15] G. Kresse and J. Furthmüller, Phys. Rev. B **54**, 11169 (1996).
[16] P. E. Blöchl, Phys. Rev. B **50**, 17953 (1994).
[17] J. P. Perdew, K. Burke, and M. Ernzerhof, Phys. Rev. Lett. **77**, 3865 (1996).
[18] X. Gonze, J.-M. Beuken, R. Caracas, F. Detraux, M. Fuchs, G.-M. Rignanese, L. Sindic, M. Verstraete, G. Zerah, F. Jollet, M. Torrent, A. Roy, M. Mikami, P. Ghosez, J.-Y. Raty, and D. Allan, Comput. Mater. Sci. **25**, 478 (2002).
[19] M. Fuchs and M. Scheffler, Comput. Phys. Commun. **119**, 67 (1999).
[20] K. A. Müller and H. Burkard, Phys. Rev. B **19**, 3593 (1979).
[21] W. Zhong and D. Vanderbilt, Phys. Rev. B **53**, 5047 (1996).
[22] A. Glazer, Acta Crystallogr., Sect. B: Struct. Crystallogr. Cryst. Chem. **28**, 3384 (1972).
[23] S. V. Halilov, M. Fornari, and D. J. Singh, Appl. Phys. Lett. **81**, 3443 (2002).
[24] N. Sai and D. Vanderbilt, Phys. Rev. B **62**, 13942 (2000).
[25] R. Shannon, Acta Crystallogr. **A32**, 751 (1976).
[26] C.-J. Eklund, C. J. Fennie, and K. M. Rabe, Phys. Rev. B **79**, 220101(R) (2009).
[27] J. H. Haeni, P. Irvin, W. Chang, R. Uecker, P. R. Y. L. Li, S. Choudhury, W. Tian, M. E. Hawley, B. Craigo, A. K. Tagantsev, X. Q. Pan, S. K. Streiffer, L. Q. Chen, S. W. Kirchoefer, J. Levy, and D. G. Schlom, Nature (London) **430**, 758 (2004).